

A rollover indicator based on a tire stiffness backstepping observer: Application to an All-Terrain Vehicle

Nicolas Bouton[◊], Roland Lenain[◊], Benoit Thuilot* and Philippe Martinet*

Abstract—Lateral rollover is the leading cause of fatal accidents in light All-Terrain Vehicles (e.g. quad bikes), especially in the agricultural area. The estimation and prediction of hazardous situations are preliminary steps in the design of active security devices. If numerous metrics have already been defined for on-road vehicles, few approaches are suitable for fast motions in a natural environment (mainly due to tire/ground contact specificity and variability). This paper proposes an algorithm dedicated to the estimation and prediction of one metric, namely Lateral Load Transfer (*LLT*), in order to anticipate rollover situations on an irregular and natural ground. It is based on a vehicle dynamic model, used jointly with a backstepping observer. It allows to take into account tire/ground contact non linearities and variability, which impact the rollover tendency. The efficiency of the metric is investigated through advanced simulations and full scale experiments on a Kymco quad bike.

I. INTRODUCTION

Serious injuries and fatal accidents induced by the use of light All-Terrain Vehicles (ATVs) do not stop raising. Indeed, ATVs have been designed to offer a good driveability, but in counterpart, their geometric characteristics may lead to an unstable and unsafe vehicle behavior on a natural ground. For instance, the US Consumer Product Safety Commission (CPSC) [9] has rated at approximately 0.7% the risk of having an accident for an ATV driver. Many studies around the world confirm the dangerousness of such vehicles and highlight the preponderant part of rollover situations in serious accidents (almost 50% of ATVs crashes as mentioned in [6] and [5]).

Therefore, the design of on-board devices improving dynamic stability of ATVs, whatever grip conditions and driver inputs, constitutes a relevant research topic. Such devices might be inspired by the numerous security systems recently developed for on-road vehicles, such as Electronic Stability Program (ESP) [3] or steering and braking control [1]. Nevertheless, the transfer of such mechanisms to an off-road context cannot be achieved straightforwardly, as some assumptions related to ground conditions (grip, regularity...) are no longer satisfied in such a context.

Since the devices to be proposed are intended to be activated only in dangerous situations, some indicators have to be designed. Several metrics have already been proposed in the literature for the detection of rollover risk, based on various principles and hypotheses, and requiring different sets of

sensors as described in [13]. Static stability indicators, as the Static Rollover Threshold (SRT) or the Static Stability Factor (SSF) [10], constitute a first category. Such indicators rely only on the vehicle geometric characteristics and do not require numerous nor expensive sensors. Unfortunately, since dynamic effects are neglected, these indicators cannot describe accurately the rollover propensity of fast vehicles moving on an irregular ground, see [19]. Therefore, dynamic indicators appear more relevant to anticipate ATVs hazardous situations. Approaches based on force-angle measurement [12], [7] or on Zero Moment Point (ZMP - proposed usually to investigate humanoid and mobile robots stability, [15], [17]) or methods dedicated to vehicle stability studies, relying either on lateral acceleration [16] or kinetic energy, may supply interesting results. However, in light ATVs context, these solutions on one hand require expensive sensors and on the other hand, are very dependent on thresholds particularly difficult to tune on a natural and variable environment.

As a result, in this paper, an approach based on the Lateral Load Transfer metric (*LLT* - such as proposed in [8]) is preferred. Indeed, the dynamic modeling aims at estimating tire/ground vertical forces with a low cost measurement system. Furthermore, the *LLT* critical threshold is quite easy to tune since the lift-off of the left or right wheels corresponds to a unitary *LLT* value.

Since ATVs are expected to move on a natural ground, the estimation of the vertical forces constitutes one of the main issues. The use of dynamic models with constant grip parameters, as in [18], does not appear relevant here, since grip conditions are actually highly variable in the intended applications. To address this difficulty, observer-based algorithms such as developed in [2] or in [14] have been preferred to a ground class selection such as developed in [4]. However, in these two examples, an extra sensor (INS or GPS sensor) which is both expensive and hardly usable on an ATV, has to be integrated. In this paper, an observer relying on a low cost sensing configuration solely composed of a gyrometer, a steering angle sensor and a Doppler radar, is proposed. It permits to estimate on-line grip conditions as well as vehicle global sideslip angle, whatever tire/ground properties. These estimations are then used to design a relevant rollover risk indicator dedicated to All-Terrain Vehicles, relying on the prediction of the *LLT*.

The paper is organized as follows: first, vehicle dynamic models (roll and yaw projections), combined with a tire model are developed, and used to derive *LLT* expression. Next, since this expression requires the knowledge of the tire cornering stiffness, an adapted backstepping observer

[◊] Cemagref, 24 av. des Landais, BP 50085, 63172 Aubière Cedex, France
nicolas.bouton and roland.lenain@cemagref.fr
* LASMEA, 24 avenue des Landais, 63177 Aubière Cedex, France
benoit.thuilot and philippe.martinet@lasmea.univ-bpclermont.fr

is designed. The proposed rollover indicator, accounting for variations in grip conditions, is then introduced. Finally, the relevancy of both the observer and the rollover indicator are demonstrated through advanced simulation (with multibody dynamic software Adams) and full scale experiments with a marketed quad bike.

II. VEHICLE MODELING

A. Dynamic models

In order to achieve on-line *LLT* computation, the global vehicle modeling depicted on Fig.1 is considered. The inputs are the vehicle velocity, the steering angle and the yaw rate, all three supplied by the low cost sensor set described in Section I. More precisely, two semi-analytical models are introduced: the yaw 2D projection (shown on Fig.1(a)), parallel to the ground plane, allows to derive some vehicle motion variables (as the lateral acceleration of the vehicle center of gravity), that are then injected into the roll 2D projection (shown on Fig.1(b)) in order to compute the *LLT*. Since ATVs are expected to move on a natural ground, sliding parameters have been introduced through sideslip angles (β , α_r , α_f) and lateral forces (F_f and F_r) depicted on Fig.1(a).

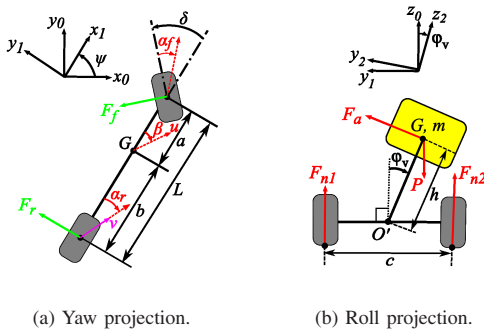


Fig. 1. Vehicle modeling.

The other notations used in this paper, and reported on Fig.1(a) and Fig.1(b), are listed below :

- $R_0(x_0, y_0, z_0)$ is the frame attached to the ground,
- $R_1(x_1, y_1, z_1)$ is the yaw frame attached to the vehicle,
- $R_2(x_2, y_2, z_2)$ is the roll frame attached to the suspended mass,
- ψ is the vehicle yaw angle,
- ϕ_v is the roll angle of the suspended mass,
- δ is the steering angle,
- v is the linear velocity at the center of the rear axle,
- u is the linear velocity at the roll center,
- a and b are the front and rear vehicle half-wheelbases,
- $L = a + b$ is the vehicle wheelbase,
- c is the vehicle track,
- h is the distance between the roll center O' and the vehicle center of gravity G ,
- I_x, I_y, I_z are the roll, pitch and yaw moments of inertia,
- $P = mg$ is the gravity force on the suspended mass m , with g denoting the gravity acceleration,
- F_{n1} and F_{n2} are the normal component of the tire/ground contact forces on the vehicle left and right sides,

- F_a is a restoring-force parametrized by k_r and b_r , the roll stiffness and damping coefficients:

$$\vec{F}_a = \frac{1}{h} (k_r \phi_v + b_r \dot{\phi}_v) \vec{y}_2 \quad (1)$$

The roll stiffness k_r and the distance h are assumed to be preliminary calibrated, as explained in section V-A. The roll damping b_r is experimentally evaluated (through a driving procedure) and the other parameters (wheelbase, weight,...) are directly measured.

B. Motion equations

In order to derive the motion equations issued from the yaw projection shown on Fig.1(a), analytical expressions of lateral forces F_f and F_r must be supplied. An accurate tire model, such as the celebrated Magic formula [11], could be considered, but it would require the knowledge of numerous parameters, hardly accessible in real-time. Therefore, a simple linear tire model has here been chosen. It can be expressed as:

$$\begin{cases} F_f = C_f(\cdot) \alpha_f \\ F_r = C_r(\cdot) \alpha_r \end{cases} \quad (2)$$

where $C_f(\cdot)$ and $C_r(\cdot)$ are respectively the front and rear tire cornering stiffnesses, greatly depending on tire/ground interaction variations. The on-line estimation of these two parameters is discussed in section III. Based on (2), the dynamic equations of the yaw model can be expressed as:

$$\begin{cases} \ddot{\psi} = \frac{1}{I_z} (-aC_f \alpha_f \cos(\delta) + bC_r \alpha_r) \\ \dot{\beta} = -\frac{1}{um} (C_f \alpha_f \cos(\beta - \delta) + C_r \alpha_r \cos(\beta)) - \dot{\psi} \\ \alpha_r = \text{atan}(\tan(\beta) - \frac{b\dot{\psi}}{u \cos(\beta)}) \\ \alpha_f = \text{atan}(\tan(\beta) + \frac{a\dot{\psi}}{u \cos(\beta)}) - \delta \\ u = \frac{v \cos(\alpha_r)}{\cos(\beta)} \end{cases} \quad (3)$$

C. Lateral load transfer computation

The general expression of the Lateral Load Transfer (*LLT*) is defined as:

$$LLT = \frac{F_{n1} - F_{n2}}{F_{n1} + F_{n2}} \quad (4)$$

A rollover situation is then detected when a unitary value of $|LLT|$ is reached, since it corresponds to the lift-off of the wheels on the same side of the vehicle. An explicit expression of *LLT*, derived from the fundamental principle of the dynamic applied to the model shown on Fig.1, is given in [4]. This expression requires the knowledge of $C_f(\cdot)$, $C_r(\cdot)$ and β which are not measured. Therefore, a backstepping observer is designed in the following section.

III. BACKSTEPPING OBSERVER

A. Observer principle

Since quad bikes are expected to move on a natural and slippery ground, actual sliding and not only pseudo-sliding, is likely to occur. A non-linear tire/ground interaction force, such as depicted in black dashed line on Fig.2, has to be considered. Since *LLT* computation is derived from linear

tire/ground model (2), it is here proposed to adapt on-line a virtual tire cornering stiffness C_e so that model (2) could reflect pseudo-sliding (in that case $C_e = C_0$) as well as actual sliding ($C_e < C_0$, see blue dashed-dotted line on Fig. 2). In addition, such an adaptation enables also to reflect variations of grip conditions.

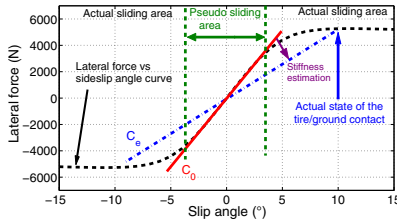


Fig. 2. Adaptation principle of the tire cornering stiffness.

As above mentioned, only yaw rate $\dot{\psi}$, rear axle linear velocity v and steering angle δ are supplied by the sensors. Based on these sole measurements, the proposed adaptation algorithm consists in a backstepping observer relying on the following assumptions:

- 1) From the few measured variables available, C_f and C_r cannot be estimated separately. Therefore, they are considered to be equal to a virtual tire cornering stiffness C_e ,
- 2) Sideslip angles α_f , α_r and β are assumed to be small (corroborated by experiments),
- 3) As a consequence, the vehicle velocity u at roll center can be considered to be equal to the rear axle one (i.e. $u \approx v$), see (3).

B. Observer design

1) *Observability*: Relying on previous assumptions, the non-linear motion equations (3) can be turned into the linear system (5):

$$\begin{cases} \dot{\tilde{\psi}} = a_{11}\tilde{\psi} + a_{12}\tilde{\beta} + b_1\delta \\ \dot{\tilde{\beta}} = a_{21}\tilde{\psi} + a_{22}\tilde{\beta} + b_2\delta \end{cases} \quad (5)$$

where: $a_{11} = \frac{-(a^2+b^2)C_e}{vI_z}$, $a_{12} = \frac{(b-a)C_e}{I_z}$, $a_{21} = -\frac{(a-b)C_e}{mv^2} - 1$,

$$a_{22} = -\frac{2C_e}{mv}, \quad b_1 = \frac{aC_e}{I_z}, \quad b_2 = \frac{C_e}{mv}$$

Then, (5) can easily be presented as a state space model:

$$\begin{cases} \dot{X} = AX + B\delta \\ Y = CX \end{cases} \quad (6)$$

with the state space vector $X = (\tilde{\psi}, \tilde{\beta})^T$ and the matrices

$$A = \begin{bmatrix} a_{11} & a_{12} \\ a_{21} & a_{22} \end{bmatrix}, \quad B = \begin{bmatrix} b_1 \\ b_2 \end{bmatrix} \quad \text{and} \quad C = [1 \quad 0]$$

Kalman observability matrix O_{obs} of system (6) is:

$$O_{obs} = \begin{bmatrix} C \\ CA \end{bmatrix} = \begin{bmatrix} 1 & 0 \\ -\frac{(a^2+b^2)C_e}{vI_z} & \frac{(b-a)C_e}{I_z} \end{bmatrix} \quad (7)$$

It can be checked that O_{obs} is a full rank matrix as soon as $a \neq b$ (which is always met on actual quad bikes) and of course $v \neq 0$. As a consequence, system (6) is observable and $\tilde{\psi}$ as well as $\tilde{\beta}$ can be estimated on-line.

2) *Backstepping approach*: The observer equations deduced from system (5) can be firstly written as:

$$\begin{cases} \ddot{\tilde{\psi}} = a_{11}(C_e) \cdot \dot{\tilde{\psi}} + a_{12}(C_e) \cdot \dot{\tilde{\beta}} + b_1(C_e) \cdot \delta \\ \ddot{\tilde{\beta}} = a_{21}(C_e) \cdot \dot{\tilde{\psi}} + a_{22}(C_e) \cdot \dot{\tilde{\beta}} + b_2(C_e) \cdot \delta \end{cases} \quad (8)$$

where $\dot{\tilde{\psi}}$ and $\dot{\tilde{\beta}}$ are respectively the observed yaw rate and sideslip angle.

In order to compute LLT , β and C_e have to be estimated from (8). To meet this aim, a backstepping approach composed of two steps is proposed. The first one consists in treating $\tilde{\beta}$ as a control input (denoted $\bar{\beta}$), to be designed to impose the following dynamic on the observed yaw rate error $\tilde{\psi}$:

$$\ddot{\tilde{\psi}} = \ddot{\tilde{\psi}} - \dot{\tilde{\psi}} = K\dot{\tilde{\psi}}, \quad K < 0 \quad (9)$$

where $\dot{\tilde{\psi}}$ is the numerical derivative of the measured yaw rate. Injecting (9) into the first equation in (8) leads to the following expression for control variable $\bar{\beta}$:

$$\bar{\beta} = \frac{\ddot{\tilde{\psi}} - K\dot{\tilde{\psi}} - a_{11}(C_e) \cdot \dot{\tilde{\psi}} - b_1(C_e) \cdot \delta}{a_{12}(C_e)} \quad (10)$$

Since $\bar{\beta}$ ensures that $\dot{\tilde{\psi}}$ converges to the actual value $\dot{\psi}$ supplied by the gyrometer, $\bar{\beta}$ can be considered as a relevant estimation of the actual global sideslip angle.

The second step in the backstepping observer consists in treating C_e as a control input to be designed to ensure the convergence of $\tilde{\beta}$ to $\bar{\beta}$. More precisely, C_e is adapted in order to impose the following dynamic on the observed sideslip angle error $\tilde{\beta}$:

$$\ddot{\tilde{\beta}} = \dot{\tilde{\beta}} - \dot{\tilde{\beta}} = G\tilde{\beta}, \quad G < 0 \quad (11)$$

Injecting (11) into the second equation in (8) leads to:

$$G\tilde{\beta} = \dot{\tilde{\beta}} - a_{21}(C_e) \cdot \dot{\tilde{\psi}} - a_{22}(C_e) \cdot \dot{\tilde{\beta}} - b_2(C_e) \cdot \delta \quad (12)$$

where $\dot{\tilde{\beta}}$ is the numerical derivative of $\tilde{\beta}$.

Finally, by injecting the expressions for a_{ij} into (12), the following virtual cornering stiffness C_e adaptation law can be obtained:

$$C_e = \frac{\dot{\tilde{\beta}} + \dot{\tilde{\psi}} - G\tilde{\beta}}{\frac{(b-a)\dot{\tilde{\psi}}}{mv^2} - \frac{2\tilde{\beta}}{mv} + \frac{\delta}{mv}} \quad (13)$$

Relying on (13), C_e can be adapted provided that $v \neq 0$ (modeling assumption) and $\delta \neq 0$ (when $\delta = 0$, it is expected that $\dot{\tilde{\psi}}$ and $\tilde{\beta}$ also converge to 0, so that the denominator in (13) is equal to 0). Since this last singularity is likely to occur, it has to be imposed that, next to neutral steering ($|\delta|$ below some steering limit), the virtual cornering stiffness is not adapted but equal to its previous value.

IV. ROLLOVER INDICATOR COMPUTATION

The proposed rollover indicator consists in the prediction of the future lateral load transfer (denoted LLT_f) over an horizon of prediction H . More precisely, the computation of LLT_f is carried out according to the algorithm described below and illustrated on Fig.3.

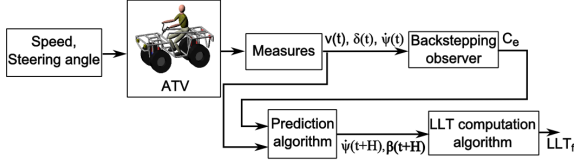


Fig. 3. LLT_f computation scheme.

At current time t :

- 1) The backstepping observer (10)-(13) is used to estimate the actual global tire cornering stiffness C_e from the three available measurements (current yaw rate $\dot{\psi}(t)$, velocity $v(t)$ and steering angle $\delta(t)$).
- 2) Expected velocity $v(t+H)$ and steering angle $\delta(t+H)$ at time $t+H$ are estimated from their numerical derivative at current time t ($\dot{v}(t)$ and $\dot{\delta}(t)$). Nevertheless, if such a prediction tends to decrease LLT_f , then the current velocity and/or steering are hold. This leads to the following expressions for the expected values:

$$v(t+H) = \begin{cases} v(t) + H\dot{v}(t) & \text{if } v(t) > 0 \text{ and } \dot{v}(t) > 0 \\ v(t) & \text{otherwise} \end{cases} \quad (14)$$

$$\delta(t+H) = \begin{cases} \delta(t) + H\dot{\delta}(t) & \text{if } \delta(t) > 0 \text{ and } \dot{\delta}(t) > 0 \\ \delta(t) + H\dot{\delta}(t) & \text{if } \delta(t) < 0 \text{ and } \dot{\delta}(t) < 0 \\ \delta(t) & \text{otherwise} \end{cases} \quad (15)$$

- 3) $\beta(t+H)$ and $\dot{\psi}(t+H)$ are derived from (3) by using $v(t+H)$, $\delta(t+H)$ and by assuming that C_e is constant on H .
- 4) Then, these future values are used to compute the future lateral load transfer LLT_f , according to the method discussed in section II-C.

Finally, if LLT_f is superior to some LLT threshold (e.g. $LLT_f = 0.8$), then corrective actions can be engaged with some anticipation.

V. RESULTS

In this section, different results are presented. First, advanced simulation results, obtained from a virtual quad bike (as depicted on Fig. 4(a)) designed with dynamic multibody software Adams, are reported. They permit to validate, from a theoretical point of view, the proposed backstepping observer as well as LLT computation and prediction algorithms on slippery ground. Then, the second part of this section presents the experimental results recorded with the Kymco Mxer 150 quad bike shown on Fig.4(b).



(a) Virtual quad bike. (b) Kymco Mxer 150.

Fig. 4. Vehicles used for simulations/experiments.

A. Advanced simulation results

1) *Simulation background*: The different characteristics of the virtual quad bike are listed in Table I. The first ones are inspired by the characteristics of a marketed ATV. The two last ones, namely the roll stiffness k_r and the distance h between the Roll Center O' and the Center of Gravity G have been calibrated according to a first simulation run with a simulated high grip ground: k_r and h have been identified, via a Newton-Raphson non-linear algorithm, in order to minimize the difference between the computed LLT and the measured LLT supplied by Adams software (more details can be found in [4]).

TABLE I
VIRTUAL QUAD BIKE PARAMETERS

Quad bike suspended mass	250 kg
I_x, I_y, I_z	45, 110, 130 $kg.m^2$
Front and rear half-wheelbases a, b	0.58, 0.7 m
Quad bike track c	0.95 m
Distance between O' and G : h	1.22 m
Roll stiffness k_r	5900 $N.m.rad^{-1}$

The path followed at $v = 21 \text{ km.h}^{-1}$ by the virtual ATV is depicted on Fig.5. The grip conditions that have been imposed correspond to a wet grass soil. The velocity, the steering angle and the yaw rate have been recorded with the software Adams at a 100Hz frequency in order to emulate sensors.

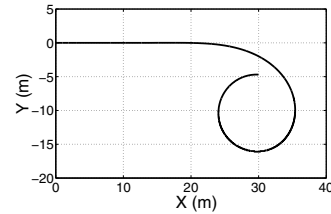


Fig. 5. Advanced simulation path.

2) *Observer performances*: Using the three measurements recorded in Adams, the backstepping observer (10)-(13) has been run in order to obtain an estimation of the virtual tire cornering stiffness. Three initial values have been successively considered ($C_0 = 40.000 \text{ N.rad}^{-1}$, $C_0 = 20.000 \text{ N.rad}^{-1}$ and $C_0 = 10.000 \text{ N.rad}^{-1}$).

Fig.6 shows the time evolution of the adapted tire stiffness C_e . From $t = 0$ to $t = 8s$, the virtual quad bike is moving according to a straight line, so that C_e is not adapted, as mentioned in section III. When the virtual quad bike enters into the curve (after $t = 8s$), then the time evolutions of the adapted tire cornering stiffness become similar whatever the initial value. This demonstrates the ability of the backstepping observer to supply a robust estimation of C_e . Moreover, the lateral forces computed by injecting the adapted C_e into model (2) are satisfactorily superposed on the measured ones provided by Adams software. This demonstrates the relevancy of the adapted tire stiffness C_e .

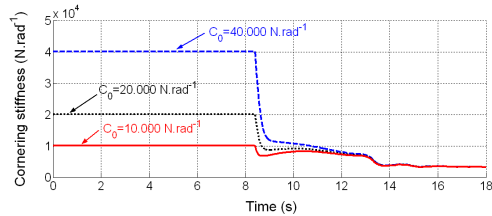


Fig. 6. Adapted tire cornering stiffness.

3) *Lateral load transfer computation*: The time evolution of the *LLT* computed with the adapted cornering stiffness C_e , when its initial value is $C_0 = 40.000 \text{ N.rad}^{-1}$, is depicted in red dashed dotted line on Fig.7. One can check that it is accurately superposed with the measured one supplied by Adams and reported in black solid line.

The green dashed line shows the time evolution of the *LLT* computed with a constant cornering stiffness $C_0 = 40.000 \text{ N.rad}^{-1}$, representative of high grip conditions (e.g. asphalt). This latter signal greatly overestimates the measured *LLT* and is stabilizing above the rollover threshold. At time $t = 18\text{s}$, the *LLT* computed with a constant C_0 presents a 15% error with respect to the *LLT* supplied by Adams. On the contrary, the *LLT* computed with the adapted C_e does not provide any erroneous information: the error with respect to the *LLT* supplied by Adams does not exceed 4%, and after transient period ($t = 18\text{s}$), the error is negligible. This demonstrates the relevancy of the backstepping observer in order to compute accurate *LLT* values when sliding occurs.

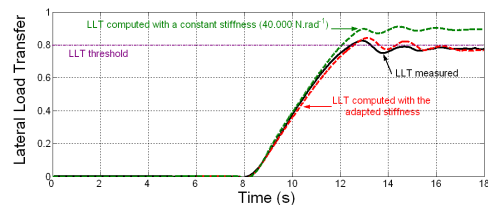


Fig. 7. Lateral load transfer comparison.

4) *Rollover risk indicator in advanced simulation*: On-line *LLT* estimation is satisfactory. However, the objective of this work is to anticipate *LLT* evolution. The proposed rollover risk indicator LLT_f , computed with an horizon of prediction $H = 0.5\text{s}$, is reported in blue dotted line on Fig.8, and compared to the measured *LLT* supplied by Adams and to the *LLT* computed on-line. It can be checked that LLT_f reaches the threshold value 0.8 one second before the measured *LLT*, which is consistent with the actuators settling time.

Since the predicted values $v(t+H)$ and $\delta(t+H)$ are computed exclusively from the first order derivatives $\dot{v}(t)$ and $\dot{\delta}(t)$, fast variations in these variables cannot be reflected. For instance, at $t=13\text{s}$, the steering angle of the virtual quad bike stops increasing because the path beyond presents a constant curvature. Since $\dot{\delta}(t)$ returns very quickly to 0, $\dot{\delta}(t+H)$ overestimates for a short time the future values of δ . Then, in this case, LLT_f is overestimated, but it might be emphasized that LLT_f cannot be underestimated, since decelerations and reductions in the steering angle are not taken into account in the prediction, see (14)-(15).

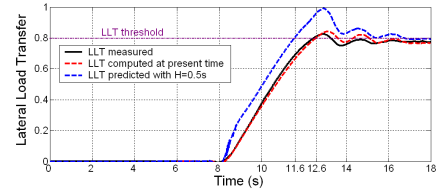


Fig. 8. Rollover risk indicator.

B. Experimental results

1) *Kymco Mxer 150 parameters*: The main parameters of the vehicle shown on Fig.4(b) have been either directly measured (mass, lengths,...) or obtained from a dedicated measurement bench (moments of inertia, position of the center of gravity). The two parameters k_r and h have been identified from preliminary tests performed on a high grip ground (asphalt), relying on the approach already mentioned in section V-A. The parameters of the Kymco Mxer 150 quad bike with the pilot are listed in Table II.

TABLE II
KYMCO MXER 150 PARAMETERS

Quad bike mass with sensors	220 kg
Pilot mass with equipment	90 kg
I_x, I_y, I_z	57, 105, 83 kg.m ²
Front and rear half-wheelbases a, b	0.66, 0.48 m
Quad bike track c	0.67 m
Distance between O' and G : h	1.32 m
Roll stiffness k_r	8600 N.m.rad ⁻¹

In order to compare the computed *LLT* with a ground truth, the quad bike has been equipped with four linear potentiometers fixed parallel to the suspensions. They enable, after a preliminary calibration, the measurement of the actual *LLT*. However, these sensors offer no insight for predicting the evolution of the *LLT* and consequently are not suitable for the anticipation of rollover risk situations (and moreover they are expensive). Experiments have been conducted on a flat ground mainly constituted of dry grass. The path that has been followed is depicted on Fig. 9 and is composed of four left half-turns. The quad bike speed was comprised between 15 and 25 km.h⁻¹.

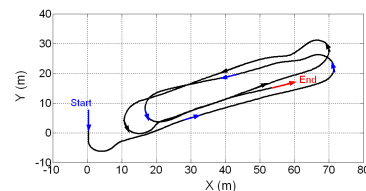


Fig. 9. Path followed during experiments.

2) *Lateral load transfer result*: Relying on the measured velocity, steering angle and yaw rate, the tire cornering stiffness has been estimated, and the lateral load transfer has then been computed and compared to the measured one on Fig.10.

When observing the four curves, it can be noticed that the computed *LLT* is satisfactorily superposed with the measured one. Moreover, in each curve the measured *LLT* crosses

the threshold value 0.8, and so does the computed *LLT*. This demonstrates the ability of the computed *LLT* to detect hazardous situations.

Finally, some negative overshoots at the end of each curve can be observed on the computed *LLT*. They correspond to an actual dynamics that cannot be measured by the sensor set: the linear potentiometers are indeed attached to the suspensions, which cannot reach total expansion instantaneously. As a consequence, the length supplied by the potentiometer is also damped and the measured *LLT* is barely equal to 1.

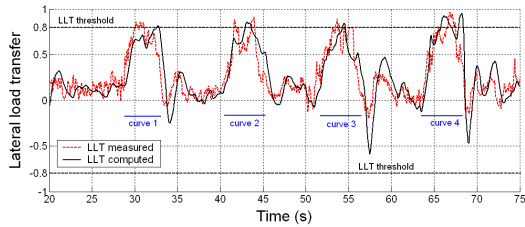


Fig. 10. Lateral load transfer comparison.

3) *Rollover risk indicator*: The rollover risk indicator, computed with an horizon of prediction $H = 0.5s$, has also been run during the above described experiment. It is reported on Fig.11 and compared to the measured *LLT*.

First, it can be observed that, as expected, the rollover risk indicator is able to anticipate hazardous situations: in each curve, the indicator crosses the threshold value 0.8 a few seconds before the measured *LLT*. This lets enough time to activate stabilization actions.

It can also be noticed that the prediction step has significantly amplified the negative overshoots observed at the end of each curve on Fig.10. As already discussed in section V-A, when the velocity and/or the steering angle are quickly varying, the prediction equations (14)-(15) may transiently overestimate the future values of these variables, and therefore the future *LLT*. However, it is not a concern, since the hazardous situation had previously been detected.

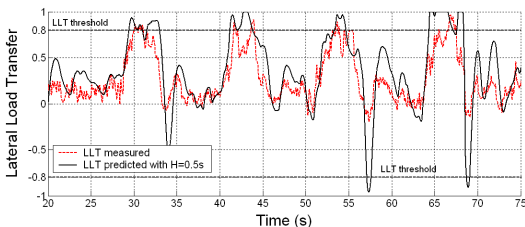


Fig. 11. Rollover risk indicator.

VI. CONCLUSION AND FUTURE WORK

This paper proposes a rollover risk indicator dedicated to light ATVs operating on a natural and slippery ground. First, a vehicle dynamic model, based on a yaw and a roll projection, has been developed. Sliding effects have been taken into account according to a simple tire/ground contact model incorporated into the yaw 2D projection. The key feature in this tire model is a virtual cornering stiffness parameter. A backstepping observer has then been proposed to estimate it on-line relying solely on a low cost sensor set.

It enables to take into account the non-linear behavior of the tire and variations in grip conditions. Based on this observer, the Lateral Load Transfer (*LLT*) can be accurately estimated and predicted. Such a prediction constitutes an interesting rollover risk indicator for the prevention of hazardous situations. Simulations, as well as experiments with a marketed quad bike, demonstrate the applicability and the relevancy of the proposed approach.

Current developments aim at integrating a nominal human behavior into the proposed algorithms. Finally, the validation of the proposed metric opens the way to the development of on-board devices for ATV dynamic stability. First research axes are focused on predictive and constrained control approaches so as to ensure the dynamic stability of ATVs.

REFERENCES

- [1] J. Ackermann, D. Odenthal, and T. Bnte. Advantages of active steering for vehicle dynamics control. In *Intern. Symposium on Automotive Technology and Automation*, Vienna, Austria, 1999.
- [2] R. Anderson and D.M. Bevy. Estimation of tire cornering stiffness using GPS to improve model based estimation of vehicle states. In *IEEE Intelligent Vehicles conference*, Las Vegas, U.S.A., 2005.
- [3] R. Bosch. *Safety, comfort and convenience systems*. Wiley, Hoboken, U.S.A., 2006.
- [4] N. Bouton, R. Lenain, B. Thuilot, and J-C. Fauroux. A rollover indicator based on the prediction of the load transfer in presence of sliding: application to an all terrain vehicle. In *Intern. Conf. on Robotics and Automation*, Roma, Italy, 2007.
- [5] CCMISA. Accidents du travail des salariés et non salariés agricoles avec des quads. Technical report, Observatoire des risques professionnels et du machinisme agricole. Paris, France, 2006.
- [6] Wisconsin department of natural resources. All terrain vehicle enforcement and safety report 2006. Technical report, 2007.
- [7] A. Diaz-Calderon and A. Kelly. Development of a terrain adaptive stability prediction system for mass articulating mobile robots. In *4th Intern. Conf. on Field and Service Robotics*, Tsukuba, Japan, 2003.
- [8] P. Gaspar, I. Szasz, and J. Bokor. Reconfigurable control structure to prevent the rollover of heavy vehicles. *Control Engineering Practice*, (13):699–711, 2005.
- [9] M.S. Levenson. All-terrain vehicle 2001 injury and exposure studies. Technical report, U.S. Consumer Product Safety Commission, 2003.
- [10] National Highway Traffic Safety Administration (NHTSA). Trends in static stability factor of passengers cars, light trucks and vans. Technical report, U.S. department of transportation, 2005.
- [11] H. B. Pacejka. *Tire and vehicle dynamics*. Society of Automotive Engineers, 2002.
- [12] E.G. Papadopoulos and D.A. Rey. A new measure of tipover stability margin for mobile manipulators. In *Intern. Conf. on Robotics and Automation*, Minneapolis, U.S.A., 1996.
- [13] S.C. Peters and K. Iagnemma. An analysis of rollover stability measurement for high-speed mobile robots. In *Intern. Conf. on Robotics and Automation*, Orlando, U.S.A., 2006.
- [14] J. Ryu, E. Rossetter, and J. Christian Berges. Vehicle sideslip and roll parameter estimation using GPS. In *6th Int. Symp. on Advanced Vehicle Control (AVEC)*, Hiroshima, Japan, 2002.
- [15] P. Sardain and G. Bessonnet. Forces acting on a biped robot. center of pressure - zero moment point. *IEEE Transactions on systems, man, and cybernetics*, 34(5):630–637, 2004.
- [16] B. Schofield, T. Hagglund, and A. Rantzer. Vehicle dynamics control and controller allocation for rollover prevention. In *Int. Conference on Control Applications*, Munich, Germany, 2006.
- [17] Z. Shiller, P.M. Mosche, and D. Rubinstein. Dynamic stability of off-road vehicles considering a longitudinal terramechanics model. In *Inter. Conf. on Robotics and Automation*, Rome, Italy, 2007.
- [18] S. Solmaz, M. Corless, and R. Shorten. A methodology for the design of robust rollover prevention controllers for automotive vehicles : Part 1-differential braking. In *45th IEEE Conference on Decision and Control*, San Diego : U.S.A., 2006.
- [19] R. Whitehead, W. Travis, D.M. Bevy, and G. Flowers. A study of the effect of various vehicle properties on rollover propensity. *SAE International*, (2004-01-2094), 2004.